

# A Causally Informed Pretraining Approach for Multimodal Foundation Models: Applications in Remote Sensing

Praveen Ravirathinam

pravirat@umn.edu

University of Minnesota, Twin Cities  
Minneapolis, Minnesota, USA

Rahul Ghosh

ghosh128@umn.edu

University of Minnesota, Twin Cities  
Minneapolis, Minnesota, USA

Ankush Khandelwal

khand035@umn.edu

University of Minnesota, Twin Cities  
Minneapolis, Minnesota, USA

Vipin Kumar

kumar001@umn.edu

University of Minnesota, Twin Cities  
Minneapolis, Minnesota, USA

## Abstract

Self-supervised learning has emerged as a powerful paradigm for pretraining foundation models using large-scale data. Existing pretraining approaches predominantly rely on masked reconstruction or next-token prediction strategies, demonstrating strong performance across various downstream tasks, including geoscience applications. However, these approaches do not fully capture the causal interplay between different geospatial and environmental variables. To address this limitation, we propose Causally Informed Variable-Step Forecasting (CI-VSF), a novel pretraining task that models forecasting as a conditional generation task, where driver variables (e.g., weather) inform the prediction of response variables (e.g., satellite imagery). We demonstrate that pretraining in such a fashion leads to enhanced performance when finetuned on both prediction (e.g., crop mapping, missing image prediction, soil moisture estimation) and forecasting (e.g., future image forecasting, soil moisture forecasting) downstream tasks when compared to other pretraining approaches. While we use remote sensing as our main application to demonstrate the efficacy of our proposed pretraining strategy over existing paradigms, it is applicable to any domain that involves known causal relationships amongst a set of variables.

## Keywords

Pretraining Tasks, Causality, Foundation Model, Remote Sensing

## 1 Introduction

In recent years, self-supervised learning methods have emerged to utilize large amounts of data for pretraining model weights using specialized pretraining tasks [16, 23]. These models, known as foundation models, have demonstrated strong performance across various downstream tasks after fine-tuning [3, 28, 30, 52]. The predominant pretraining strategies come from either masked reconstruction [10, 18] or next-token prediction [1]. Beyond these, other approaches such as contrastive learning [21, 39], student-teacher models [17] have also been explored for pretraining.

Masked reconstruction (MR)-based pretraining involves self-supervised tasks where a portion of the input data is hidden (masked), and the model is trained to reconstruct the original data. This style of pretraining has shown great progress in the vision domain (where parts of the image are masked [18]) and in the language domain (where words from sentence are masked [10]). In the geoscience

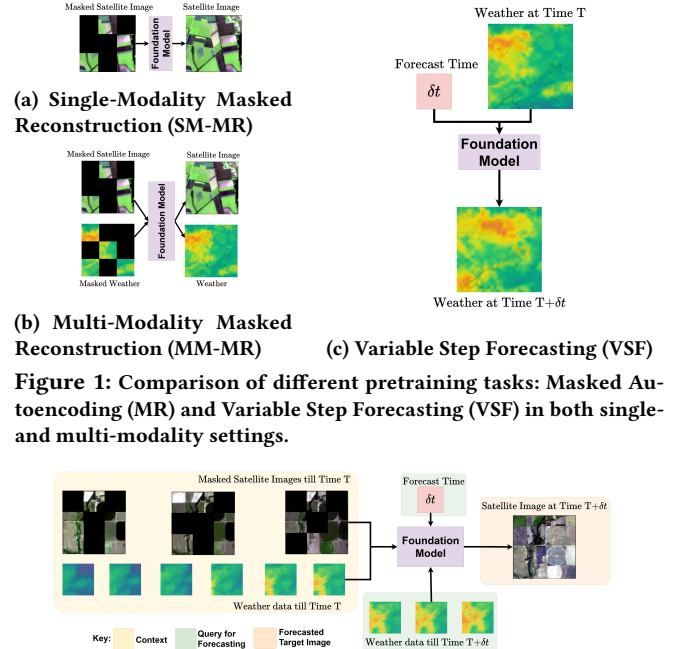


**Figure 1: Comparison of different pretraining tasks: Masked Autoencoding (MR) and Variable Step Forecasting (VSF) in both single- and multi-modality settings.**

domain, masked reconstruction has been used extensively in the building of remote sensing foundation models [6, 8, 22, 32, 47]. In such models, parts of the satellite image are masked, and the objective is to reconstruct the entire satellite image (denoted by Figure 1a). Utility of finetuning such models has been demonstrated for numerous *prediction based downstream tasks* where the aim is to estimate or infer current or past variables using available data. Examples of such tasks include flood inundation mapping, wild-fire scar mapping, cloud removal, urban semantic segmentation mapping, scene classification etc. [8, 22, 44]. Researchers improved this pretraining task by adding multiple modalities (MM) to the reconstruction objective (shown in Figure 1b), where instead one modality, multiple masked modalities would be used to create a common embedding, from which all modalities would be reconstructed. Finetuning models trained with such a pretraining task

has been shown to lead to improvements in scene classification and crop field classification [36, 47].

Next-token prediction-based pretraining involves self-supervised tasks where, given a sequence of data, the model is trained to predict the next or subsequent data points. This style of pretraining has been used in language modeling (where given a sequence of words the model learns to predict the next word[46]) most notably GPT[1]. In the geoscience domain, next token prediction style of pretraining has been used in the climate/weather foundation models [13, 37, 38, 41]. Here, given a series of masked or unmasked climate variables, the objective is to estimate these climate variables at a random future timestamp (see Figure 1c). Models pretrained in this variable step forecasting (VSF) fashion have shown great performance in *forecasting based downstream tasks*, where the aim is to predict future variables based on past observations. Examples of such tasks include precipitation forecasting, hurricane trajectory tracking, sea surface temperature prediction.

In geosciences, there is often a complex interplay between different variables i.e., one set of variables (drivers) influence the other set of variables (response). For example, weather (driver) influences the vegetation growth (response) which can be observed by a satellite. In such scenarios none of the two pre-training paradigms (MR and VSF) fully utilize the relationship between these sets of variables for learning robust representations. For example, consider foundation models for remote sensing applications. Here, VSF based pre-training solely using satellite data is not adequate because change in satellite imagery in a region strongly depends on how weather interacts with that region. In other words, satellite imagery alone does not have enough information to estimate future states without weather. Furthermore, just using MR pretraining does not allow for capturing of temporal patterns in land cover change to be effectively included during pre-training.

In this paper, we propose a novel pre-training task for building foundation models that leverages the dependence (causality) between variables. This pre-training task, which we call Causally Informed Variable Step Forecasting (CI-VSF), models forecasting as a conditional generation task where conditioning is governed by the driver variables (e.g. weather) and the task is to predict the response variables (e.g. satellite images). While we use remote sensing as our main application to demonstrate the efficacy of this pretraining strategy over existing paradigms (MR and VSF), it is applicable to any domain that involves known causal relationships amongst a set of variables. Specifically, we propose forecasting of satellite imagery with weather context as a novel pre training task for building remote sensing foundation models (shown in Figure 2), i.e using a series of satellite imagery and weather data up till a future date, our task is to estimate the satellite image in the future. This method of pretraining captures the causal relationship between variables, and the resulting embeddings lead to better performance on both prediction and forecasting based downstream tasks compared to existing methods of pretraining.

To summarize, our key contributions are listed below:

- We propose Causally Informed Variable-Step Forecasting (CI-VSF), a pretraining objective that leverages causal-guided principles to train models while preserving the causal dependencies between modalities, unlike existing approaches such as standard multimodal masked reconstruction or variable-step forecasting.

- We show the efficacy of our pretraining task by training a foundation model in stages, beginning with multimodal masked reconstruction and ending with Causally Informed Variable-Step Forecasting.
- We demonstrate that embeddings when trained in our proposed stage-wise approach can outperform models trained with the baseline methods when fine-tuned for a range of spatiotemporal downstream applications such as soil moisture related tasks (prediction and forecasting), pixel wise crop mapping (prediction), and spectral imagery based tasks (prediction and forecasting)
- We release the code and model used to public (Link)

## 2 Related Work

Increased availability and ease of access to large scale satellite data has motivated the development of deep learning models that use this data to perform various geoscience tasks such as land cover mapping [15, 25], wildfire mapping [35, 43, 51], crop yield prediction [26, 49], flood forecasting [5] etc. This has led to a large number of geoscience foundation models[4, 6, 9, 17, 20, 22, 31–34, 41]. Most of these foundation models can be placed into one of two groups based on the data they use : (1) weather-climate [37, 38] that are typically used for weather forecasting or climate modeling and (2) spectral data from remote sensing satellites [8, 22, 31, 36, 47] that are largely used for identifying land-use land-cover change dynamics. The most common pretraining task in geoscience has been reconstruction of spectral imagery. To enrich the embedding created, varying amounts of the input spectral image are masked, making the reconstruction task of the entire image harder leading to better embeddings [8]. However, simple reconstruction embeddings capture just that particular image and might not be suited for downstream tasks that rely on multi temporal contexts such as crop mapping or land cover land use change. To solve this, previous works included multiple timestamps in their input, however some of these methods stacked these images together [22], thus removing the temporal aspect. However, some methods added a timestamp positional embedding so that the model has a sense of time [8, 24]. This led to moderate success in handling downstream tasks that require multi temporal contexts. Another common pre-training task is forecasting of imagery. Typically, this pretraining task has been used in weather related foundation models and not in spectral imagery based foundation models. Foundation models created using masked forecasting has shown great success in weather related downstream tasks [38, 41]. To enrich the embeddings created, these works add variable future time forecasting, i.e vary the amount of time into the future the model needs to forecast, which was achieved by including an embedding for delta time [37]. Other variants of foundation models include diffusion models that incorporate more information such as geographic location, time of year, country etc [24]. Other class of geoscience foundation models include contrastive learning based foundation models, where multiple modalities are aligned to form similar embeddings, which are then used for downstream tasks[17, 48].

## 3 Architecture

Our architecture follows a heavy encoder and lightweight decoder format. Keeping our decoder lightweight forces richer embeddings from encoder, suitable for downstream tasks. As mentioned before, we incorporate multiple modalities (spectral imagery and weather)

in pretraining our architecture. Figure 3 shows CI-VSF’s architecture. For the forecasting-based pre-training task, it is essential for architecture to capture spatiotemporal nature of satellite data, temporal nature of weather data, and most importantly, the causality.

**Satellite image Encoder/Decoder:** We use a shared Vision Transformer (ViT) to extract spatial features from spectral imagery across timestamps. ViT have been shown to be effective in the presence of high masking [18], even in geoscience contexts [22]. The ViT converts each image into a patch grid of embeddings, incorporating patch positional information. This results in a series of spectral image embeddings on unmasked patches for each timestamp. Since our input is an image series, we propose using a shared ViT across timestamps, leading to a robust encoder, that is capable of embedding images from all timestamps.

**Weather Encoder** Due to the coarse spatial resolution of weather data, typically for each image location, we have one weather data point value per timestamp. Thus we use a sequence-to-sequence Unidirectional LSTM to encode the weather data. The LSTM based approach showed higher accuracy over the transformer based approaches when trying to solely reconstruct masked weather. The LSTM generates weather embeddings for each timestamp, which are then subsampled to match input image timestamps, similar to WSTAT [40], called temporal embedding matching.

**Timestamp/Delta Encoder** For temporal information we incorporate day of year (DOY) using a shared linear layer with tanh activation, creating DOY embeddings for each timestamp. Additionally, we create another series that corresponds the number of days in between the images, i.e the delta in timestamps. We generate embeddings for these time delta between images using a separate linear layer. The DOY embeddings provide temporal context, while delta embeddings, shown useful in forecasting tasks [37], informs the model about forecast distance.

**Multimodal Sequence Encoder** From the previous steps we have spatial, weather, and DOY embedding series. Since all these series are of the same length, we add them all along the temporal dimension to create the multimodal embedding series. We use a transformer with forward-only attention to extract the spatio-temporal information from this multimodal embedding series, analyzing embedding patches from the same spatial location across timestamps. Further we add forward only attention (causal) in transformer, i.e the temporal embeddings created are not bidirectional in nature. This feature makes sure there is no information leakage from future timestamp information to previous timestamps embeddings. The resulting embedding series  $Emb_{STW} = [Emb_{:t_1}^{t_1}, \dots, Emb_{:t_C}^{t_C}]$  can be used for downstream tasks, with flexibility in embedding selection.

**Forecaster** Since our embeddings are constructed using forward-only attention, we use each of the embeddings in  $Emb_{STW}$  to forecast an image in its respective future. For each embedding  $Emb_{:t_i}^{t_i}$ , the forecaster uses the weather embeddings  $Emb_w^{t_j}$  as well as the temporal embeddings  $Emb_t^{t_j}$  and the delta embeddings to generate the embeddings  $Emb^{t_j}$  of the forecast timestamp  $t_j$ . By incorporating weather data leading up to a particular date, we can make more informed estimates about how the land cover might appear, as weather patterns play a significant role in shaping the landscape over time. We combine the four embeddings through addition and

feed it to a series of linear and activation layers that forms our forecaster. The objective of these layers is to morph the embeddings from current timestamp to the future timestamp before passing them to the MLP decoder to get the satellite image forecast.

For all but last embeddings in the series  $Emb_{STW}$ , we forecast the next time-step, i.e  $t_1$  of the input series would be used to forecast the image at  $t_2$ ,  $t_2$  would be used to forecast  $t_3$  and so on (In a similar fashion to the Causal Language Modeling pretraining task used in Large Language Models [1]). For the last embedding  $Emb_{:t_C}^{t_C}$  we forecast the  $K$ ’th time-step, which is  $K-C$  days into the future. This  $K$  is a variable and is sampled for each training instance in a batch, thus the name variable-step forecasting (VSF). This method enables the model to predict future images based on current image embeddings and weather information up to the forecast date, acknowledging weather’s impact on land cover.

**Decoder** Following this stage, we repopulate these embeddings in their respective unmasked positions in the timestamps and zero out the masked patches to pass to the decoder, as done by most methods in transformer based autoencoder methods [18, 22]. We use a light-weight MLP decoder (similar to the one used in ViT) to ensure that the main focus of the model is to create strong encoder to capture the best information. Similar, to the encoder, we have a shared decoder that performs the operations on each timestamp using the same weights. The decoder maps the embeddings to the spectral image space and reshapes the output to match the required size of the spatiotemporal stack.

## 4 Pretraining

As mentioned before, our proposed pretraining task is forecasting of satellite imagery using multimodal data in a causally informed fashion, a pretraining task that varies significantly from the traditional single modality reconstruction. Our proposed approach can be trained using the architecture described above in a direct shot, i.e initialise and update all layers at once. However, this may not be the best way to ensure that the  $Emb_{STW}$  embeddings capture causal information, as that is the ultimate aim of our proposed approach. To ensure this information capture, we propose a phase wise pretraining process. Specifically we propose 2 phases of pretraining, where the first phase focuses on getting information from each modality and the second phase focuses on capturing the causal relationship between modalities in the embedding.

**Phase 1: Masked Reconstruction** Our architecture consists of several components, each serving a distinct purpose. The ViT encoder/decoder maps images to and from embedding space and can be trained separately via masked satellite image reconstruction. Similarly, the Weather encoder embeds weather data and also can be trained using a masked autoencoder approach with a Unidirectional LSTM. These steps yield embeddings for both spectral imagery and weather data. Next, we integrate the multimodal sequence encoder, training it to reconstruct the entire satellite image series by masking embeddings instead of images, strengthening its sequence-learning capability. This establishes a baseline for the  $Emb_{STW}$  embedding series (through addition with the weather embeddings). While this series captures spatial and temporal patterns, it lacks capturing causal relationships. To validate this, we use it as a baseline for downstream task fine-tuning. Finally, in Phase 2, we introduce a forecaster to infuse causal relationships.

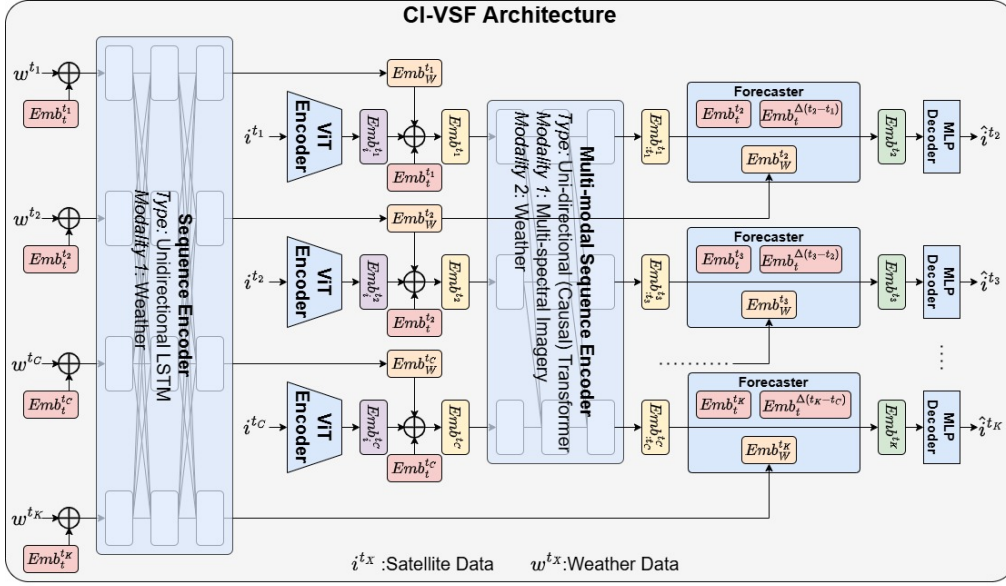


Figure 3: Causally Informed Variable step Forecasting (CI-VSF) Architecture diagram

**Phase 2: Forecasting** From section 3, the forecaster consists of linear layers, and although simple, its role is crucial: it translates embeddings from the input timestamp space to the forecasted timestamp space. Achieving this transformation within a few layers is challenging, so the model will seek to learn this relationship from other components, which would be provided by the weather data. Using weather data, along with current, timestamp, and delta embeddings, the forecaster generates future embeddings. Given the limited layers, all embeddings adjust to capture relevant cross-modal information for forecasting. For instance, heavy rainfall leads to fuller lakes, while increased sunlight accelerates vegetation growth. Repeating this process over various samples embeds land growth and change dynamics into the model’s representations. Without weather data, the model lacks a relationship to learn, making forecasting significantly harder. This no-weather variant serves as an additional baseline for downstream tasks.

To summarize, our proposed pretraining task is to predict a spectral image in the future (response) using a series of spectral images in the past (context) along with the weather till that future date (query). We call this pretraining task as Causally Informed Variable step Forecasting (CI-VSF), where the model is expected to forecast  $k$  steps into the future. To ensure that relationship across modalities is captured in the embeddings, we adopt a two phase pretraining process. Our hypothesis is that this extra knowledge infusion would help greatly in downstream tasks that rely on land growth and change dynamics such as crop prediction, land cover land use change, etc. A schematic of the stagewise pretraining can be found in appendix A.1. We mask out patches in the spectral imagery and weather data in all the stages to lead to better embeddings, which we describe in a future section (Sec 5.2).

## 5 Dataset

### 5.1 Data Sources

Our spectral imagery data comes from Sentinel imagery [11] and our weather data is from ERA5 land analysis data [19]. We chose these two sources due to their temporal resolutions and more importantly their availability globally from 2021. We randomly sampled around 10000 locations across land areas globally. Each location is of size 128x128 Sentinel pixels and for spectral imagery we collected all images for that region in that year. Due to missing data and improper coverage of some regions, the number of Sentinel samples from each region would vary. For example, regions in well covered regions such as US, might have upto 70 image instances in a year for that region, whereas regions like India (which is not as well covered) would have 40 image instances. For each instance, we collect six bands namely (B2, B3, B4, B8, B9, B12), which have shown to be the most useful in land cover related tasks and have been used in other works [22]. For each image instance, we also collect the day of the year it came from, thus forming a series with values from 1 to 365 and a length the same as the number of image instances for that location. Though ERA5 data source consists of various bands that are useful for land cover related tasks we chose 5 bands that are the primary weather drivers, namely (temperature 2m min, temperature 2m max, total precipitation sum,  $u$  component of wind 10m,  $v$  component of wind 10m). ERA5 data is available at a daily temporal resolution and a spatial resolution of 11k meters.

To summarise, for each location our data comprises of:

- **Spectral Imagery Series:** A series of Sentinel2 Imagery each of 6 bands and of shape 128x128. Length of this series depends on coverage of the location.
- **Weather Data Series:** A series of ERA5 Land data of 5 bands and of shape 1x1, with a series length of 365 (one per day). The reason behind having only one pixel value from weather data is due to its coarse resolution (11km) compared to the area covered by our Sentinel patch (1.28km x 1.28km)

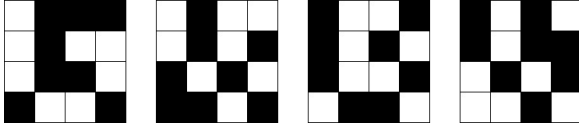


Figure 4: Example of 50 percent spatiotemporally uniform masking on a 4x4 4 image timeseries

- **Day of Year Series:** A series of the day of the year number for each spectral image in the series. The length of this series is same as the spectral imagery series.

## 5.2 Masking

Since we have a spatiotemporal input and architecture, we adopt a spatiotemporally uniform masking method, i.e, masking that is fair both spatially and temporally. In our unique masking strategy, there are an equal number of masked patches per timestamp as well as an equal number of masked patches per spatial patch location along the temporal axis. Figure 4 shows an example of such masking for a image series of 4 4x4 grids with 50% masking. From the Figure, we can see that in each timestamp image there are 8 patches masked and focusing on a particular patch location along the temporal dimension we notice that 2 patches are available. This ensures that all temporal patch series that can be created from unmasked patches at each spatial location would be of same length, easing the implementation of temporal components. Also the shared vision transformer will also have same number of outputs per timestamp due to same number of unmasked patches per timestamp.

## 6 Experimental Evaluation

### 6.1 Comparative Pretraining Frameworks

In our experiments, we evaluate the effectiveness of CI-VSF by comparing with several representative foundation modeling frameworks. We model these frameworks by varying the choices for input and pretraining tasks from existing works, as described below.

- **SM-MR:** Single Modality Masked Reconstruction (SM-MR) with satellite data as input and MR as the pretraining task. This is the most common setup used in existing remote sensing foundation models (e.g., [8, 22, 44]).
- **MM-MR:** MultiModal Masked Reconstruction (MM-MR) with satellite and weather data as input series and MR as pretraining task. This represents the foundation models that use multiple modalities but still do masked reconstruction (eg. [36, 47])
- **SM-VSF:** Single Modality Variable step Forecasting (SM-VSF) with the satellite data as input series and VSF as pretraining task.

It is important to note that the goal of the paper is not to release a new foundation model but show efficacy of our novel pre-training strategy for building foundation models. We are aiming to show how a causally guided pretraining task embeds causal information, which leads to superior performance on down stream tasks where capturing this causality matters compared to standard pretraining tasks. As a result, we will not be comparing ourselves with other existing foundation models directly (which are trained with millions of images and heavy gpu resources [8, 22]) but rather implement their frameworks (architecture design, pretraining task, etc.) on our dataset to ensure fair comparison and convince researchers in the future to use our approach for pretraining of their remote

sensing based foundation models. Note that in our setup the above frameworks can be implemented by changing the inputs and the loss functions, without significant architecture changes. Though MM-MR also uses multi modal data, due to the pretraining task of masked reconstruction, the causal relationship between modalities is not captured in the embeddings and in turn hurts its performance on downstream tasks.

### 6.2 Implementation and Pretraining Details

For the pretraining phase, we choose an input series length of 6 images, and selected a random image after the 6th image as the final image to forecast. Since our input series length is 6, we can create multiple samples from one location, i.e one location’s data can result in multiple input series. After splitting the 10000 sampled locations in 60-20-20 split and created numerous samples in each split, We used 50000 image series for training, 10000 images series for validation, and 10000 for testing. We also use 50% spatiotemporally uniform masking for both forecasting and reconstruction based pretraining. We use a patch size of 8 for the vision transformer and a hidden dimension size of 256. Models were trained with a learning rate of 0.0001 on 4 A100 Nvidia GPUs using Adam Optimizer and Mean Squared Error loss. A batch size of 128 was used and all frameworks were trained for 800 epochs each. If the framework required a forecasting phase, it was trained during the final 300 epochs of the total 800 epochs.

All models were trained till convergence. MM-MR reached lower mean squared loss compared to SM-MR, and CI-VSF reached a lower mean square error loss compared to SM-VSF. While the output images produced by SM-MR and MM-MR were quite clean, the images produced by SM-VSF were blurry. CI-VSF was also able to create clean and consistent images, while showing good forecasting performance. For more details please refer to appendix section A.2

## 7 Results: Soil Moisture Tasks

In this section, we compare the performance of fine-tuned models on soil moisture related tasks, specifically soil moisture forecasting and soil moisture prediction.

### 7.1 Soil Moisture Forecasting

**Dataset and Problem Setting:** Soil moisture forecasting plays a important role in the remote sensing domain, enabling various applications such as optimizing crop management, planning irrigation schedules, and improving drought monitoring and mitigation strategies [12, 45]. In this downstream task, we aim to evaluate the ability of models to forecast soil moisture estimates. Specifically, we seek to predict soil moisture at a given location at an arbitrary future time based on past satellite imagery, weather and soil moisture observations. We focus on 6 Sentinel tiles (T11SKA, T10SEJ, T14SKC, T15TUH, T16SBF, T14RQT) regions (geographic locations shown in Appendix Figure 12) and obtain the corresponding Sentinel2, ERA5 and SMAP (‘soil\_moisture\_am’ band) values for those regions at their optimal temporal and spatial resolutions. Our goal is to forecast SMAP (‘soil\_moisture\_am’ band) values at some point in the future using past context.

To estimate a soil moisture value in the future, the inputs we provide are satellite image time series, weather data till that future

**Table 1: Comparison of models fine-tuned from different pretraining tasks on soil moisture forecasting downstream task. Table reports average Mean Absolute Error (MAE) of forecasted SMAP values for different forecast day ranges. In the test region soil moisture ranged from 0.062 to 0.4998 with a mean of 0.2134 and standard deviation of 0.0997, providing context for interpreting the values below**

Soil Moisture Forecasting Downstream Task		
Future Forecast Day Range	SM-VSF	CI-VSF
0 - 25 days	0.0406	<b>0.0179</b>
25 - 50 days	0.0429	<b>0.0184</b>
50 - 100 days	0.0549	<b>0.0189</b>
More than 100 days	0.0678	<b>0.0204</b>

date and past soil moisture values. We use a input interval of 6 satellite images and predict the soil moisture value at a 7th timestamp in the future. Each tile is split into 100 grids and a 60-20-20 train-val-test split is done, ensuring no overlap in regions. Multiple samples are generated from each grid, and after preprocessing, we retain 1800 samples for training, 400 for validation, and 400 for testing. To enhance model generalization, we ensure a diverse distribution of forecast range (i.e. the number of days into the future for which forecasts are made), allowing the model to learn both short-term and long-term forecasting patterns. Due to the forecasting related nature of this task, it would be inappropriate to finetune with the SM-MR and MM-MR embeddings, as these methods are not designed for extrapolating into the future. A decoding head for forecasting is appended and finetuned using Mean Absolute Error loss. Encoder is kept fixed. For more architecture and implementation details please refer to Appendix Section A.3.

**Performance:** We train a model for both the SM-VSF and CI-VSF settings using all tiles and a diverse range of forecast day (i.e. varying number of days into the future for forecasting). To compare the performance of these models systematically, we compare predictions made across different forecast ranges in the test grids, reported in Table 1. From Table 1, in short forecast ranges (i.e. less than 25 days) both SM-VSF and CI-VSF finetuned models are able to forecast soil moisture quite well with a moderate difference between the two. However, when we move to larger forecast ranges, we can see a big jump in the performance of CI-VSF finetuned model compared to SM-VSF’s finetuned model. Even though as the forecast range increases, errors of both models go up, the errors by the SM-VSF model go up significantly higher compared to CI-VSF’s model. This can be attributed to the fact that the CI-VSF model is able to capture the causal relationships between weather satellite imagery and past soil moisture values better than the SM-VSF counterpart, leading to a performance boost especially as we forecast farther into the future.

## 7.2 Soil Moisture Estimation

**Dataset and Problem Setting:** Estimation of Soil Moisture at current timestamp using radar imagery has been a topic of interest in the remote sensing community[2, 27, 42]. Typically, multiple sources of data including satellite data, radar data, weather data, depth data, etc. are used to estimate in-situ measurements from their site where groundtruth readings are available. In our downstream task, we aim to emulate this task and demonstrate how a pretraining task that captures causal relationships in its embeddings is better

**Table 2: Comparison of models fine-tuned from different pretraining tasks on the downstream task of soil moisture prediction. Mean Absolute Errors for each experiment setting is shown. In the Test region soil moisture values ranged from 0.0669 to 0.4727 with a mean value of 0.2177 and standard deviation of 0.0972, providing context for interpreting the values below**

Soil Moisture Prediction Finetuned Models				
TEST Tile	SM-MR	MM-MR	SM-VSF	CI-VSF
In region Testing: Train on 6 tiles, Test on all 6 tiles				
All	0.0615	0.0458	0.0483	<b>0.0282</b>
Cross-Region Testing: Train on 5 tiles, Test on the 6th.				
T11SKA	0.1113	0.0847	0.1121	<b>0.0695</b>
T15TUH	0.1283	0.1365	0.1181	<b>0.0834</b>
T14SKC	0.1159	0.1275	0.1312	<b>0.0958</b>
T16SBF	0.0821	0.0631	0.0895	<b>0.0544</b>
T10SEJ	0.1003	0.0718	0.1011	<b>0.0587</b>
T14RQT	0.0815	0.0579	0.0658	<b>0.0558</b>

for the task of soil moisture estimation. From the same 6 Sentinel tiles used in the soil moisture forecasting problem, we obtain the Sentinel-2 satellite data and ERA5 weather data to serve as our input modalities and the ‘soil\_moisture\_am’ band from SMAP to serve as our groundtruth for soil moisture[29].

In our problem setting, the input would be a time series of either one or multiple modalities with the goal to estimate the soil moisture at that location for each timestamp. We use a timeframe of 6 satellite images here and aim to estimate the soil moisture at each timestamp. For sample generation, like the previous section, each tile is split into 100 grids and a 60-20-20 train-val-test split is done, and after preprocessing, we retain 1800 samples for training (300 from each tile), 600 for validation (100 from each tile), and 600 for testing (100 from each tile). Due to the prediction related nature of this task, models from all 4 pretraining tasks are finetuned. A decoding head for prediction is appended and finetuned using Mean Absolute Error loss. Encoder is kept fixed. For more architecture and implementation details please refer to Appendix Section A.4.

**Performance:** The performance of finetuned models on this task are presented in Table 2. The first experiment conducted was training using samples from all tiles and testing on samples from the test grids of each tile. From this in region sample testing, we can see CI-VSF’s finetuned model outperforms other models quite significantly. To explore robustness of learned representations, we also explore cross region testing. In this setting, during finetuning, samples from 1 tile are hidden and during testing, models are tested samples from that hidden tile. For example, models are trained on the 1500 samples from 5 tiles (T10SEJ, T14SKC, T15TUH, T16SBF, T14RQT) and tested on the 100 test samples from the hidden tile (T11SKA). We run this setting hiding each tile one at a time, shown in the lower portion of Table 2. From these results, CI-VSF’s model is able to perform cross region soil moisture estimation better than other models in all tiles, showing that embeddings from CI-VSF are able to capture causality and retain this information even when tested on regions not included in finetuning. This highlights how causally informed pretraining strategies help in downstream tasks.



**Table 3: Comparison on downstream task of crop mapping across the pretraining tasks finetuned using only 2018 data. Classwise scores shown in Appendix table 6**

2019 Test 11 class average F1 Scores				
	SM-MR	MM-MR	SM-VSF	CI-VSF
Average	0.5331	0.5789	0.5731	<b>0.6233</b>

## 8 Results: Pixel Wise Crop Mapping

In this section, we explore the performance on the downstream task of pixel wise crop mapping.

**Dataset and Problem Setting:** Pixel wise crop mapping has been a topic of great study in the remote sensing community with numerous applications. Our data for finetuning comes from Sentinel2 and ERA5 land data for the region of the T11SKA Sentinel tile in the California Central Valley, a region rich in various crop classes and has been used for crop type mapping in various other works[14, 15, 40] from the years 2018 and 2019. Like other works, we get our labels for this region from the Cropland Data Layer(CDL), an annually released land cover map for the entire continuous US by the USDA. A diagram of the CDL labels and geographic location of T11SKA tile can be seen in Appendix Figure 7.

In this problem setting, we use 10 spectral images (biweekly from May to Sept) and weather data (within that timeframe) to predict pixel wise crop labels at a 10m resolution. Similar to WSTAT [40], we adopt a grid based training method, by splitting the entire region into train, validation and test grids and also follow their preprocessing steps including combination and erosion. Note that the number of timestamps passed in the downstream task is different from the number passed during pretraining highlighting the temporal flexibility of our architecture. Due to the prediction related nature of this task, models from all 4 pretraining tasks are finetuned. A decoding head for semantic segmentation is appended and finetuned using cross entropy loss. Encoder is kept fixed. For more architecture and implementation details please refer to Appendix Section A.5.

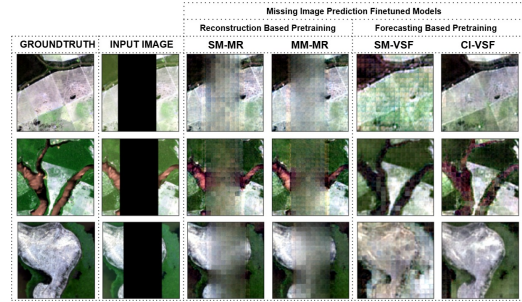
**Performance** Table 3 compares the performance of CI-VSF and other pretraining approaches when finetuned for crop mapping task. Though finetuning is done using 2018 data, testing is done on 2019 data, assessing the robustness of the approaches. We can see that CI-VSF performs better than other variants (Classwise scores shown in Appendix table 6). We also observe that MM-MR performs better than SM-MR, which is because inclusion of weather in input is in general better for crop mapping task [40], however MM-MR lacks capturing the relationship between modalities, thus its inferior performance when compared to CI-VSF. Finally, the ability of CI-VSF’s embeddings to generalize across years after finetuning indicates that the embeddings have captured crucial information that go beyond what is just present in spectral imagery.

## 9 Results: Spectral Imagery Tasks

In this section, we explore some spectral imagery related downstream tasks, specifically missing image prediction and forecasting of future satellite image.

### 9.1 Missing Image Prediction

**Dataset and Problem Setting:** With the vast amount of satellite imagery being captured on a daily basis, corrupted or missing

**Figure 5: Comparison of predictions for 50% missing values across finetuned models from different pretraining tasks.**

data is an occurring phenomenon. In some cases, the areas of missing/corrupted data is provided as a mask, but in other cases this mask is not provided, making it hard to clean or filter data, thus leaving researchers to use these corrupted images in their work[7, 50]. In this downstream task, we aim to fill these corrupted/missing values in the absence of these masks, i.e the methods have no access/information as to which pixels are corrupted, making it a very relevant downstream task.

In this problem setting, we aim to use a spatiotemporal spectral imagery series in which one or more images have missing data and predict those missing values. For our dataset, we chose to sample a new 1000 locations globally, similar to how our base dataset was created. We then did a 60-20-20 training-validation-test split and used patch series from the 600 patches for finetuning. We ensured that there is no overlap in regions across the 1000 newly sampled patches. We chose a input series length of 6, and varied the amount of missing values in input to make the task more challenging. Due to the prediction related nature of this task, models from all 4 pretraining tasks are finetuned. Decoder is reinitialised and finetuned using Mean Square Error loss. Encoder is kept fixed. For more architecture and implementation details please refer to Appendix Section A.6.

**Performance:** Table 4 compares the Mean Squared Errors across the various finetuned models. We can see that as the percentage of missing values increases, the MSE values go up, which can be expected due to the task getting harder. However, we can note that the CI-VSF pretrained models have significantly lower MSE values when compared to MR variants. We also note that CI-VSF performs the best across all missing value percentages, with the error not rising as much as the other variants. This is because the causal nature of CI-VSF helps in filling in the missing values. We also observe that the difference between SM-MR and MM-MR is not very high, thus furthering our hypothesis that MM-MR method of pretraining does not effectively capture the relationship between the different modalities of data.

In Figure 5 we compare some output images from our 50 percent missing values experiment across the four methodologies. Each row corresponds to a test sample, and a common trend across rows is that finetuned models pretrained using MR based methodologies do not fill the missing portions very well. In the first row, we can see that SM-VSF has added some false greenness but CI-VSF has not, showing that due to weather information, CI-VSF knows that growth has not occurred. Row 2 depicts a dried up river bed, but

**Table 4: Comparison on missing image prediction downstream task across models finetuned from different pretraining tasks. Mean Squared Errors on various levels of missing image percentages shown**

Missing Image Prediction Finetuned Models				
% Missing	SM-MR	MM-MR	SM-VSF	CI-VSF
50%	792.68	788.94	362.02	<b>326.43</b>
70%	820.46	814.75	394.32	<b>337.79</b>
90%	826.23	820.43	404.32	<b>343.88</b>

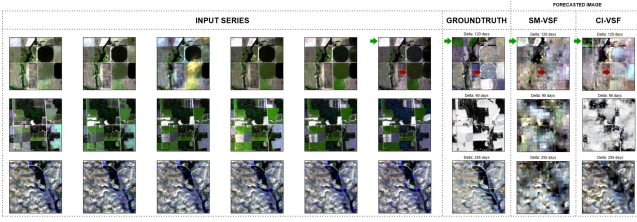


**Figure 6: Image Forecast Downstream Task comparison.** Row 1 depicts a crop field, Green arrows depict regions of growth, and Red arrows depict regions of harvest, CI-VSF captures both these phenomena better than SM-VSF. Row 2 depicts a case where CI-VSF adds snowfall accurately compared to SM-VSF. Row 3 depicts a case where CI-VSF does not change land cover due to terrain but SM-VSF adds false greenness. Please zoom for better viewing. Larger version of this image is available in Appendix Figure 11

one can observe that SM-VSF fills the image with a wet river bed, whereas CI-VSF correctly estimates the dried up bed, once again proving that weather information has helped here. In the final row, we see a case where SM-VSF did not green up the region, but CI-VSF did, which once again is a result of causal embeddings.

## 9.2 Future Image Forecasting

**Dataset and Problem Setting:** In this downstream task, we would aim to estimate a satellite image in the future given past data. Some applications where this task setting is applicable includes estimating how crops will grow in future (use the forecasted growth to calculate crop yield), predicting unavailable image due to revisit interval of satellite, etc. This downstream task is actually very similar to our pretraining objective, except here we focus only on the prediction of the last image of the series and do not include any masking of satellite imagery. So we can use the same training, validation and testing regions used in pretraining. However instead of using all images for finetuning, we randomly sample 1000 for training and 500 for testing and validation each. Like the soil moisture forecasting task, due to the forecasting related nature of this task, it would be inappropriate to finetune with the SM-MR and MM-MR embeddings. Decoder is reinitialised and finetuned using Mean Square Error loss. Encoder is kept fixed. For more architecture and implementation details please refer to Appendix Section A.7.

**Performance:** Table 5 compares the finetuned models performance on the image forecasting task, reporting average mean squared errors for different forecast ranges. We can observe that in the low forecast range (i.e 0 to 25 days into the future), CI-VSF finetuned model performs moderately better than the SM-VSF finetuned counterpart. However, as we increase the forecast day range, we can see the difference in performance between the two models

**Table 5: Comparison of models fine-tuned from different pretraining tasks on the downstream image forecasting task. The table reports the Mean Squared Error (MSE) of forecast image for different forecast day ranges**

Image Forecasting Downstream Task		
Forecast Day Range	SM-VSF	CI-VSF
0 - 25 days	340.13	<b>237.21</b>
25 - 50 days	591.54	<b>278.83</b>
50 - 100 days	1093.62	<b>358.23</b>
More than 100 days	1112.84	<b>457.27</b>

diverge, with significant differences in beyond 100 day forecasts. This can be attributed to the fact that the encoder of CI-VSF has learnt the causal relationship between weather and satellite imagery and so is able to forecast well into the future with minimal finetuning. To highlight this further, some specific examples in the high forecast range are explored.

Figure 6 shows a comparison of the forecasted images from these finetuned models, i.e SM-VSF and CI-VSF, on 3 independent examples. Each row correspond to a sample, with the first 6 images corresponding to the satellite component of the input series to the model, the weather component is not shown in the image but is passed along with the satellite component (as shown in Figure 3). Row 1 depicts an example of a crop field, with the final forecast image being 120 days following the 6th image in the input series. From the groundtruth image, we see that harvest has occurred in the circular fields and growth has happened in the top left corner field. Comparing the forecasted images from SM-VSF and CI-VSF, we can see that CI-VSF is able to capture both the harvest and the growth of the crops whereas SM-VSF is not able to capture these changes, showing that causal land cover dynamics have been captured by CI-VSF. Row 2 shows another example of a crop field, with the forecast image being 90 days in the future. We can see from the groundtruth image that 90 days later snow is present in the field, which is captured by CI-VSF but not SM-VSF, whose prediction shows a faded green field. This illustrates the ability of CI-VSF to capture the relationship between precipitation and temperature (i.e., precipitation during cold winter days can fall as snow). One can also notice that evergreen regions within the forecasted image of CI-VSF have less snowfall when compared to the fields, showing capture of terrain information. This is further reflected in Row 3, where a mountainous region is depicted and the forecast image 255 days in future. We can see that even after 255 days there is not much change in the region, which is correctly captured by our method (CI-VSF), illustrating terrain information capture, whereas SM-VSF seems to add some false greenness. We further observe that all images from the forecast of SM-VSF appear blocky, inspite of long periods of training. This is because the model is unable to forecast images without weather information.

## 10 Discussion and Conclusion

In this paper, we proposed a novel pretraining task for building foundation models, which we call Causally Informed Variable Step Forecasting (CI-VSF). Using remote sensing as a case study, we showed that the embeddings produced by our approach capture



causal dependencies between weather and satellite data (i.e. captures the impact of weather on the land cover). These embeddings result in improved fine-tuned models for downstream tasks compared to the embeddings produced by traditional pretraining methods. Specifically, we observed significant performance gains in soil moisture-related tasks (soil moisture prediction and soil moisture forecasting), pixel-wise crop mapping, and spectral imagery-based tasks (missing image prediction and future image forecasting).

Note that the weather is not the sole determining factor for the land cover, as it can be impacted by human actions (e.g., urbanization) or other natural factors not directly covered by weather (e.g., damage to crops via pest infestation). Such downstream tasks will not benefit from our approach. That said, there are numerous other applications where our methodology could have a significant impact. Some examples include: Wildfire tracking and progression forecasting (Wildfire spread is influenced by wind speed and land dryness, both of which are determined by weather conditions), Crop yield forecasting (Weather patterns directly impact crop growth, and can help mitigate potential losses), Snow cover melt forecasting (snowmelt behavior is based on temperature and precipitation patterns can aid water resource management).

Future work will include the development of a full-scale foundation model on a scale much larger than used in this study with only 50,000 samples, and make it available for use by the community in a wide range of geoscience applications.

## References

- [1] Josh Achiam, Steven Adler, Sandhini Agarwal, Lama Ahmad, Ilge Akkaya, Florencia Leoni Aleman, Diogo Almeida, Janko Altmenschmidt, Sam Altman, Shyamal Anadkat, et al. 2023. Gpt-4 technical report. *arXiv preprint arXiv:2303.08774* (2023).
- [2] Hamed Adab, Renato Morbidelli, Carla Saltalippi, Mahmoud Moradian, and Gholam Abbas Fallah Ghalhari. 2020. Machine learning to estimate surface soil moisture from remote sensing data. *Water* 12, 11 (2020), 3223.
- [3] Muhammad Awais, Muzammal Naseer, Salman Khan, Rao Muhammad Anwer, Hisham Cholakkal, Mubarak Shah, Ming-Hsuan Yang, and Fahad Shahbaz Khan. 2025. Foundation Models Defining a New Era in Vision: a Survey and Outlook. *IEEE Transactions on Pattern Analysis and Machine Intelligence* (2025).
- [4] Favyen Bastani, Piper Wolters, Ritwik Gupta, Joe Ferdinando, and Aniruddha Kembhavi. 2023. Satlaspretrain: A large-scale dataset for remote sensing image understanding. In *Proceedings of the IEEE/CVF International Conference on Computer Vision*. 16772–16782.
- [5] Roberto Bentivoglio, Elvin Isufi, Sebastian Nicolaas Jonkman, and Riccardo Taormina. 2022. Deep learning methods for flood mapping: a review of existing applications and future research directions. *Hydrology and Earth System Sciences Discussions* 2022 (2022), 1–50.
- [6] Keumgang Cha, Junghoon Seo, and Taekyung Lee. 2023. A billion-scale foundation model for remote sensing images. *arXiv preprint arXiv:2304.05215* (2023).
- [7] Baili Chen, Hongwei Zheng, Lili Wang, Olaf Hellwich, Chunbo Chen, Liao Yang, Tie Liu, Geping Luo, Anming Bao, and Xi Chen. 2022. A joint learning Im-BiLSTM model for incomplete time-series Sentinel-2A data imputation and crop classification. *International Journal of Applied Earth Observation and Geoinformation* 108 (2022), 102762.
- [8] Yezhen Cong, Samar Khanna, Chenlin Meng, Patrick Liu, Erik Rozi, Yutong He, Marshall Burke, David Lobell, and Stefano Ermon. 2022. Satmae: Pre-training transformers for temporal and multi-spectral satellite imagery. *Advances in Neural Information Processing Systems* 35 (2022), 197–211.
- [9] Cheng Deng, Tianhang Zhang, Zhongmou He, Qiyuan Chen, Yanyuan Shi, Yi Xu, Luoyi Fu, Weinan Zhang, Xinbing Wang, Chenghu Zhou, et al. 2024. K2: A foundation language model for geoscience knowledge understanding and utilization. In *Proceedings of the 17th ACM International Conference on Web Search and Data Mining*. 161–170.
- [10] Jacob Devlin. 2018. Bert: Pre-training of deep bidirectional transformers for language understanding. *arXiv preprint arXiv:1810.04805* (2018).
- [11] Matthias Drusch, Umberto Del Bello, Sébastien Carlier, Olivier Colin, Veronica Fernandez, Ferran Gascon, Bianca Hoersch, Claudia Isola, Paolo Laberinti, Philippe Martimort, et al. 2012. Sentinel-2: ESA's optical high-resolution mission for GMES operational services. *Remote sensing of Environment* 120 (2012), 25–36.
- [12] Amaury Dubois, Fabien Teytaud, and Sébastien Verel. 2021. Short term soil moisture forecasts for potato crop farming: A machine learning approach. *Computers and Electronics in Agriculture* 180 (2021), 105902.
- [13] Zhihan Gao, Xingjian Shi, Hao Wang, Yi Zhu, Yuyang Bernie Wang, Mu Li, and Dit-Yan Yeung. 2022. Earthformer: Exploring space-time transformers for earth system forecasting. *Advances in Neural Information Processing Systems* 35 (2022), 25390–25403.
- [14] Rahul Ghosh, Praveen Ravirathinam, Xiaowei Jia, Ankush Khandelwal, David Mulla, and Vipin Kumar. 2021. Calcrop21: A georeferenced multi-spectral dataset of satellite imagery and crop labels. In *2021 IEEE International Conference on Big Data (Big Data)*. IEEE, 1625–1632.
- [15] Rahul Ghosh, Praveen Ravirathinam, Xiaowei Jia, Chenxi Lin, Zhenong Jin, and Vipin Kumar. 2021. Attention-augmented spatio-temporal segmentation for land cover mapping. In *2021 IEEE International Conference on Big Data (Big Data)*. IEEE, 1399–1408.
- [16] Jie Gui, Tuo Chen, Jing Zhang, Qiong Cao, Zhenan Sun, Hao Luo, and Dacheng Tao. 2024. A Survey on Self-supervised Learning: Algorithms, Applications, and Future Trends. *IEEE Transactions on Pattern Analysis and Machine Intelligence* (2024).
- [17] Xin Guo, Jiangwei Lao, Bo Dang, Yingying Zhang, Lei Yu, Lixiang Ru, Liheng Zhong, Ziyuan Huang, Kang Wu, Dingxiang Hu, et al. 2024. Skysense: A multimodal remote sensing foundation model towards universal interpretation for earth observation imagery. In *Proceedings of the IEEE/CVF Conference on Computer Vision and Pattern Recognition*. 27672–27683.
- [18] Kaiming He, Xinlei Chen, Saining Xie, Yanghao Li, Piotr Dollár, and Ross Girshick. 2022. Masked autoencoders are scalable vision learners. In *Proceedings of the IEEE/CVF conference on computer vision and pattern recognition*. 16000–16009.
- [19] Hans Hersbach, Bill Bell, Paul Berrisford, Shoji Hirahara, András Horányi, Joaquín Muñoz-Sabater, Julien Nicolas, Carole Peubey, Raluca Radu, Dinand Schepers, et al. 2020. The ERA5 global reanalysis. *Quarterly Journal of the Royal Meteorological Society* 146, 730 (2020), 1999–2049.
- [20] Danfeng Hong, Bing Zhang, Xuyang Li, Yuxuan Li, Chenyu Li, Jing Yao, Naoto Yokoya, Hao Li, Pedram Ghamisi, Xiuping Jia, et al. 2024. SpectralGPT: Spectral remote sensing foundation model. *IEEE Transactions on Pattern Analysis and Machine Intelligence* (2024).
- [21] Ashish Jaiswal, Ashwin Ramesh Babu, Mohammad Zaki Zadeh, Debapriya Banerjee, and Fillia Makedon. 2020. A survey on contrastive self-supervised learning. *Technologies* 9, 1 (2020), 2.
- [22] Johannes Jakubik, Sujit Roy, C. E. Phillips, Paolo Fraccaro, Denys Godwin, Bianca Zadrozny, Daniela Szwareman, Carlos Gomes, Gabby Nyirjesy, Blair Edwards, Daiki Kimura, Naomi Simumba, Linsong Chu, S. Karthik Mukkavilli, Devyani Lambhate, Kamal Das, Ranjini Bangalore, Dario Oliveira, Michal Muszynski, Kumar Ankur, Muthukumaran Ramasubramanian, Iksha Gurung, Sam Khallaghi, Hanxi, Li, Michael Cecil, Maryam Ahmadi, Fatemeh Kordi, Hamed Alemohammad, Manil Maskey, Raghu Ganti, Kommy Weldemariam, and Rahul Ramachandran. 2023. Foundation Models for Generalist Geospatial Artificial Intelligence. *arXiv:2310.18660* [cs.CV]. <https://arxiv.org/abs/2310.18660>
- [23] Longlong Jing and Yingli Tian. 2020. Self-supervised visual feature learning with deep neural networks: A survey. *IEEE transactions on pattern analysis and machine intelligence* 43, 11 (2020), 4037–4058.
- [24] Samar Khanna, Patrick Liu, Linqi Zhou, Chenlin Meng, Robin Rombach, Marshall Burke, David B Lobell, and Stefano Ermon. 2023. Diffusionsat: A generative foundation model for satellite imagery. In *The Twelfth International Conference on Learning Representations*.
- [25] Nataliia Kussul, Mykola Lavreniuk, Sergii Skakun, and Andrii Shelestov. 2017. Deep learning classification of land cover and crop types using remote sensing data. *IEEE Geoscience and Remote Sensing Letters* 14, 5 (2017), 778–782.
- [26] Kentaro Kuwata et al. 2015. Estimating crop yields with deep learning and remotely sensed data. In *2015 IEEE international geoscience and remote sensing symposium (IGARSS)*. IEEE, 858–861.
- [27] Chang Suk Lee, Eunha Sohn, Jun Dong Park, and Jae-Dong Jang. 2019. Estimation of soil moisture using deep learning based on satellite data: A case study of South Korea. *GIScience & Remote Sensing* 56, 1 (2019), 43–67.
- [28] Jiajia Li, Mingle Xu, Lirong Xiang, Dong Chen, Weichao Zhuang, Xunyu Yan, and Zhaojian Li. 2024. Foundation models in smart agriculture: Basics, opportunities, and challenges. *Computers and Electronics in Agriculture* 222 (2024), 109032.
- [29] Qingliang Li, Ziyu Wang, Wei Shangguang, Lu Li, Yifei Yao, and Fanhua Yu. 2021. Improved daily SMAP satellite soil moisture prediction over China using deep learning model with transfer learning. *Journal of Hydrology* 600 (2021), 126698.
- [30] Yuxuan Liang, Haomin Wen, Yuqi Nie, Yushan Jiang, Ming Jin, Dongjin Song, Shirui Pan, and Qingsong Wen. 2024. Foundation models for time series analysis: A tutorial and survey. In *Proceedings of the 30th ACM SIGKDD conference on knowledge discovery and data mining*. 6555–6565.
- [31] Fan Liu, Delong Chen, Zhangqingyun Guan, Xiaocong Zhou, Jiale Zhu, Qiaolin Ye, Liyong Fu, and Jun Zhou. 2024. Remoteclip: A vision language foundation model for remote sensing. *IEEE Transactions on Geoscience and Remote Sensing* (2024).

- [32] Siqi Lu, Junlin Guo, James R Zimmer-Dauphinee, Jordan M Nieusma, Xiao Wang, Parker VanValkenburgh, Steven A Wernke, and Yuankai Huo. 2024. AI foundation models in remote sensing: A survey. *arXiv preprint arXiv:2408.03464* (2024).
- [33] Gengchen Mai, Chris Cundy, Kristy Choi, Yingjie Hu, Ni Lao, and Stefano Ermon. 2022. Towards a foundation model for geospatial artificial intelligence (vision paper). In *Proceedings of the 30th International Conference on Advances in Geographic Information Systems*. 1–4.
- [34] Utkarsh Mall, Cheng Perng Phoo, Meilin Kelsey Liu, Carl Vondrick, Bharath Hariharan, and Kavita Bala. 2023. Remote sensing vision-language foundation models without annotations via ground remote alignment. *arXiv preprint arXiv:2312.06960* (2023).
- [35] Guruprasad Nayak, Varun Mithal, Xiaowei Jia, and Vipin Kumar. 2018. Classifying multivariate time series by learning sequence-level discriminative patterns. In *Proceedings of the 2018 SIAM International Conference on Data Mining*. SIAM, 252–260.
- [36] Vishal Nedungadi, Ankit Karirya, Stefan Oehmcke, Serge Belongie, Christian Igel, and Nico Lang. 2024. MMEarth: Exploring multi-modal pretext tasks for geospatial representation learning. In *European Conference on Computer Vision*. Springer, 164–182.
- [37] Tung Nguyen, Johannes Brandstetter, Ashish Kapoor, Jayesh K Gupta, and Aditya Grover. 2023. ClimaX: A foundation model for weather and climate. *arXiv preprint arXiv:2301.10343* (2023).
- [38] Jaideep Pathak, Shashank Subramanian, Peter Harrington, Sanjeev Raja, Ashesh Chattopadhyay, Morteza Mardani, Thorsten Kurth, David Hall, Zongyi Li, Kamyar Aizzazadenesheli, et al. 2022. Fourcastnet: A global data-driven high-resolution weather model using adaptive fourier neural operators. *arXiv preprint arXiv:2202.11214* (2022).
- [39] Alec Radford, Jong Wook Kim, Chris Hallacy, Aditya Ramesh, Gabriel Goh, Sandhini Agarwal, Girish Sastry, Amanda Askell, Pamela Mishkin, Jack Clark, et al. 2021. Learning transferable visual models from natural language supervision. In *International conference on machine learning*. PMLR, 8748–8763.
- [40] Praveen Ravirathinam, Rahul Ghosh, Ankush Khandelwal, Xiaowei Jia, David Mulla, and Vipin Kumar. 2024. Combining Satellite and Weather Data for Crop Type Mapping: An Inverse Modelling Approach. In *Proceedings of the 2024 SIAM International Conference on Data Mining (SDM)*. SIAM, 445–453.
- [41] Johannes Schmude, Sujit Roy, Will Trojak, Johannes Jakubik, Daniel Salles Civitarese, Shradha Singh, Julian Kuehnert, Kumar Ankur, Aman Gupta, Christopher E Phillips, Romeo Kienzler, Daniela Szwarcman, Vishal Gaur, Rajat Shinde, Rohit Lal, Arlindo Da Silva, Jorge Luis Guevara Diaz, Anne Jones, Simon Pfrendschuh, Amy Lin, Aditi Sheshadri, Udaysankar Nair, Valentine Anantharaj, Hendrik Hamann, Campbell Watson, Manil Maskey, Tsengdar J Lee, Juan Bernabe Moreno, and Rahul Ramachandran. 2024. Prithvi WxC: Foundation Model for Weather and Climate. *arXiv:2409.13598 [cs.LG]* <https://arxiv.org/abs/2409.13598>
- [42] IP Senanayake, I-Y Yeo, JP Walker, and GR Willgoose. 2021. Estimating catchment scale soil moisture at a high spatial resolution: Integrating remote sensing and machine learning. *Science of The Total Environment* 776 (2021), 145924.
- [43] Seyd Teymooor Seydi, Mahdi Hasanlou, and Jocelyn Chanussot. 2022. Burnt-Net: Wildfire burned area mapping with single post-fire Sentinel-2 data and deep learning morphological neural network. *Ecological Indicators* 140 (2022), 108999.
- [44] Xian Sun, Peijin Wang, Wanxuan Lu, Zicong Zhu, Xiaonan Lu, Qibin He, Junxi Li, Xuee Rong, Zhuojun Yang, Hao Chang, et al. 2022. RingMo: A remote sensing foundation model with masked image modeling. *IEEE Transactions on Geoscience and Remote Sensing* 61 (2022), 1–22.
- [45] Rodrigo Togneri, Diego Felipe dos Santos, Glauber Camponogara, Hitoshi Nagano, Gilliard Custódio, Ronaldo Prati, Stênio Fernandes, and Carlos Kamienski. 2022. Soil moisture forecast for smart irrigation: The primetime for machine learning. *Expert Systems with Applications* 207 (2022), 117653.
- [46] Hugo Touvron, Thibaut Lavril, Gautier Izacard, Xavier Martinet, Marie-Anne Lachaux, Timothée Lacroix, Baptiste Rozière, Naman Goyal, Eric Hambro, Faisal Azhar, et al. 2023. Llama: Open and efficient foundation language models. *arXiv preprint arXiv:2302.13971* (2023).
- [47] Gabriel Tseng, Ruben Cartuyvels, Ivan Zvonkov, Mirali Purohit, David Rolnick, and Hannah Kerner. 2023. Lightweight, pre-trained transformers for remote sensing timeseries. *arXiv preprint arXiv:2304.14065* (2023).
- [48] Yi Wang, Conrad M Albrecht, Nassim Ait Ali Braham, Chenying Liu, Zhitong Xiong, and Xiao Xiang Zhu. 2024. Decoupling common and unique representations for multimodal self-supervised learning. In *European Conference on Computer Vision*. Springer, 286–303.
- [49] Jiaxuan You, Xiaocheng Li, Melvin Low, David Lobell, and Stefano Ermon. 2017. Deep gaussian process for crop yield prediction based on remote sensing data. In *Proceedings of the AAAI conference on artificial intelligence*, Vol. 31.
- [50] Hongwei Zhao, Sibio Duan, Jia Liu, Liang Sun, and Louis Reymondin. 2021. Evaluation of five deep learning models for crop type mapping using sentinel-2 time series images with missing information. *Remote Sensing* 13, 14 (2021), 2790.
- [51] Yi Zhao, Jiale Ma, Xiaohui Li, and Jie Zhang. 2018. Saliency detection and deep learning-based wildfire identification in UAV imagery. *Sensors* 18, 3 (2018), 712.
- [52] Ce Zhou, Qian Li, Chen Li, Jun Yu, Yixin Liu, Guangjing Wang, Kai Zhang, Cheng Ji, Qiben Yan, Lifang He, et al. 2024. A comprehensive survey on pretrained

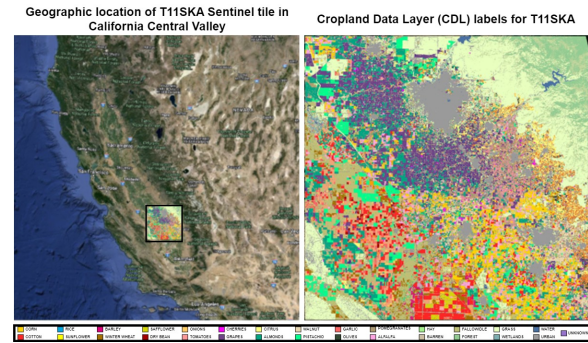


**Figure 7: Geographic location of the T11SKA Sentinel Tile and its corresponding CDL labels. Each color in the CDL image corresponds to a land cover class.**

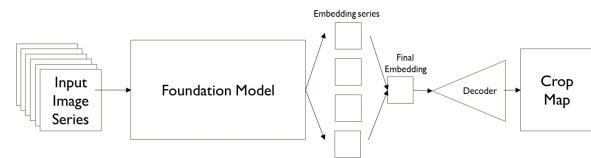


**Figure 8: Layout of architecture for downstream task of crop mapping**

foundation models: A history from bert to chatgpt. *International Journal of Machine Learning and Cybernetics* (2024), 1–65.

## A Appendix

### A.1 Pretraining Stages

Figure 9 depicts a diagrammatic representation of the 2 phase stage wise pretraining we propose to ensure that our models’s embeddings are able to capture the interaction between modalities.

### A.2 Pretraining Results

Figure 10 depicts a comparison of SM-MR and MM-MR on some test samples. We can observe that MM-MR does better than SM-MR, but only so slightly. We can notice small differences in each row (lack of greenness, blocky pixels, slight false greenness). Even on comparing Mean Squared error between the two approaches there was not a big difference.

### A.3 Soil Moisture Forecasting

**Region of Analysis:** Figure 12 depicts the geographic locations of the 6 tiles used in the soil moisture experiments.

**Architecture and Implementation details:** To capture the past context soil moisture values in the architecture, we use a unidirectional LSTM and add the corresponding hidden state embeddings with their counterparts in the  $Emb_{STW}$  (We follow the same strategy of how we combine weather and satellite imagery embeddings). This series will then be used to forecast a value in the future based on the forecast day for that sample (delta T). Since the output is a single value for each sample time series, we use a series of linear layers with Relu on the final embedding to lower the dimension to a single value. Since we are finetuning, we freeze the weights of the encoder and update only the weights of the decoder and the

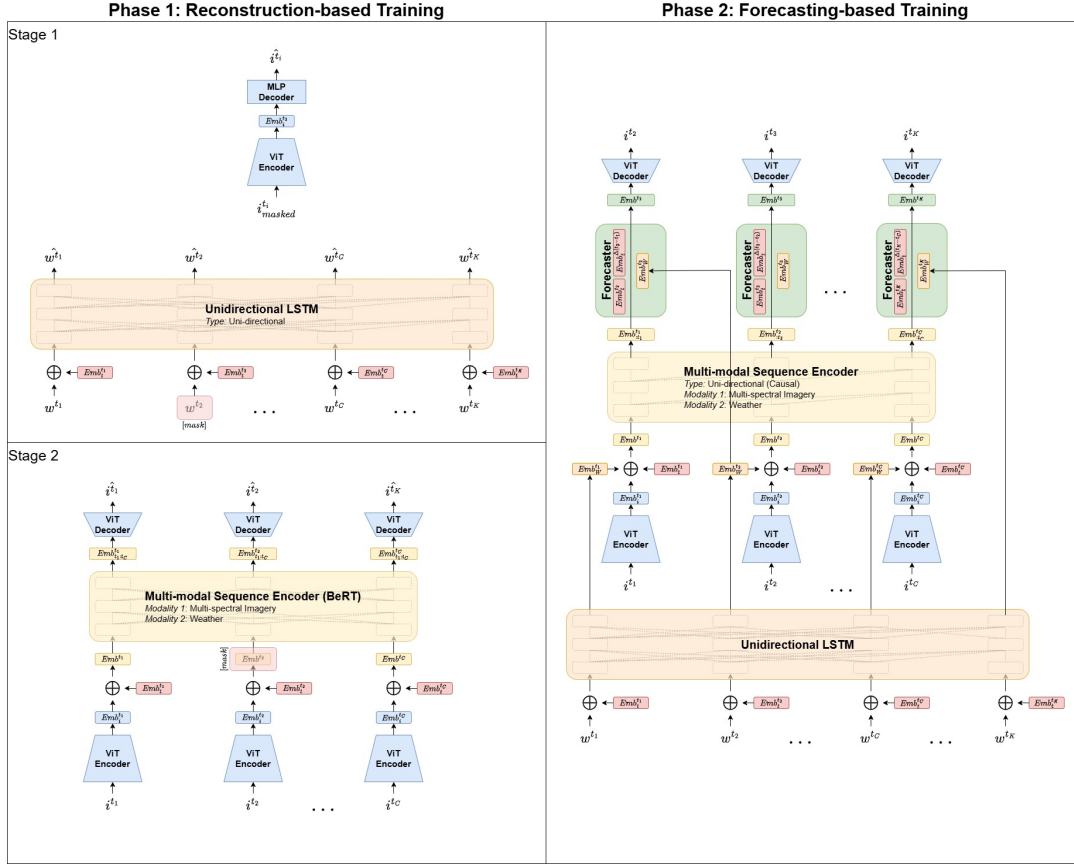


Figure 9: A diagrammatic representation of the proposed stages of pretraining

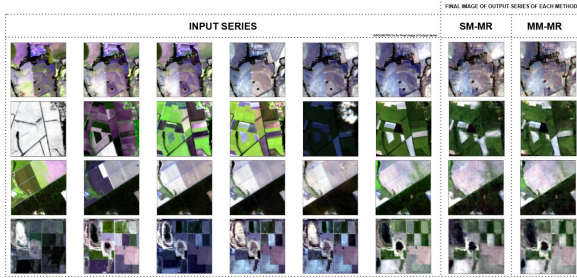


Figure 10: A comparison of MM-MR and SM-MR on some test samples. As can be seen, MM-MR is slightly better than SM-MR.

soil moisture LSTM for 50 epochs using Mean Absolute Error Loss and AdamW Optimizer with a learning rate of 0.0001.

#### A.4 Soil Moisture Prediction

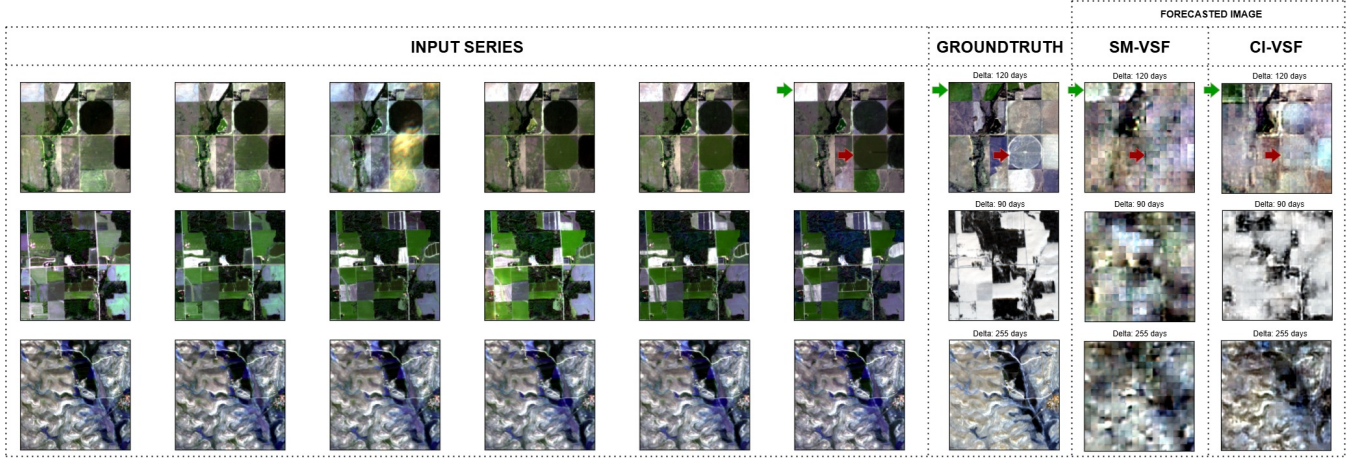
**Architecture and Implementation details** Since our output is a single value for each timestamp in the series, we use a series of shared linear layers with Relu following each Embedding in the series to get to our output at each timestamp. For each sample, since the images were sampled at random temporally across the entire year the resulting satellite image series has uneven time intervals. This leads us to also pass the day of year series as input as well. All

Table 6: Comparison on downstream task of crop mapping across the pretraining tasks finetuned using only 2018 data.

Crop Class	2019 Test Classwise F1 Scores			
	SM-MR	MM-MR	SM-VSF	CI-VSF
Corn	0.4135	0.4717	0.4489	<b>0.5708</b>
Cotton	0.8346	0.8403	0.9055	<b>0.9125</b>
Winter Wheat	0.1156	0.0770	0.1043	<b>0.1777</b>
Tomatoes	<b>0.7680</b>	0.7637	0.7223	0.7341
Grapes	0.7398	0.7502	0.7447	<b>0.7543</b>
Almonds	0.3851	<b>0.4386</b>	0.2073	0.2990
Walnut	0.0238	0.1417	0.4494	<b>0.5384</b>
Pistachio	0.5070	0.6734	0.6200	<b>0.7003</b>
Alfalfa	0.6892	<b>0.7271</b>	0.7072	0.7057
Grass	0.7760	0.8436	0.7715	<b>0.8445</b>
Urban	0.6111	<b>0.6408</b>	0.6229	0.6191
Average	0.5331	0.5789	0.5731	<b>0.6233</b>

models were finetuned for 70 epochs. Like the previous task, the encoder weights were frozen and only the shared linear heads were finetuned using Mean Absolute Error Loss and AdamW optimizer with a learning rate of 0.0001.





**Figure 11: Image Forecast Downstream Task comparison.** Row 1 depicts a crop field where, Green arrows depict regions of growth, and Red arrows depict regions of harvest, CI-VSF captures both these phenomena better than SM-VSF. Row 2 depicts a case where CI-VSF adds snowfall accurately compared to SM-VSF. Row 3 depicts a case where CI-VSF does not change land cover due to terrain but SM-VSF adds false greenness. Larger version available in Appendix Figure



**Figure 12: Geographic location of the 6 Sentinel tiles used in the soil moisture experiments**

### A.5 Pixel Wise Crop Mapping

**Region of Analysis:** Figure 7 depicts the Cropland Data Layer (CDL) labels and the region of analysis (Sentinel Tile T11SKA) for our crop mapping downstream task. As can be seen our region of analysis lies in the heart of the California Central Valley and contains numerous crop classes.

**Architecture and Implementation details:** To perform crop mapping we would need an architecture that gives us a pixel wise output, in particular, we would need a decoder that takes the embedding series given by the foundation model encoder, i.e  $Emb_{STW}$ , using it to construct a pixel wise classification map. To map this embedding series to a pixel wise map, we follow an attention based approach, similar to WSTAT[40]. This strategy assigns a weightage to each timestamp and does an aggregated sum to form a multitemporal attention-based embedding. This multitemporal embedding is then acted on by a series of upscaling and convolution layers with activation, and an output Linear layer to form a pixel wise map. Figure 8 depicts the general layout of the architecture used for the crop mapping downstream task. The embedding series mentioned would correspond to the series  $Emb_{STW}$ , i.e the output

series of the encoder. In all methods (CI-VSF, SM-MR, etc.) the encoder weights are fixed from the respective pretraining task and only the attention mechanism and decoder layers are finetuned. All models finetuning is done with only 2018 data for 40 epochs using Cross Entropy Loss and Adam optimizer with a learning rate of 0.0001.

**Performance:** Classwise F1 score performance on the test set can be seen in Table 6. We can see a good improvement in classes where weather influences crop growth directly, such as Corn and Walnut.

### A.6 Missing Image Prediction

**Architecture and Implementation details** Since our output is a series of images, we can use the same architecture as the pretraining model. However, we freeze the encoder and reinitialise the decoder weights to random values and update only these layers. To simulate missing data, we would zero out large blocks from the image and pass an input series with the blacked out images to the model. For our study, we chose to blacken out 2 images per series, both with a particular percentage of missing values. Consequently, we would pass a series of input images with one or more timestamps having missing data, and we would ask our architecture to reconstruct the entire series, but take only the mean squared loss on the timestamps with missing values, using those loss values for backpropagation. Models were finetuned for 30 epochs with Adam Optimiser and a learning rate of 0.0001.

### A.7 Future Image Forecasting

**Architecture and Implementation details:** Since we are forecasting imagery in the future, we can keep the overall architecture the same as during the pretraining (figure 3 for the CI-VSF variant) but reinitialise the decoder weights. We used an input series of length 6, kept the encoder fixed and only finetune the decoder layers for just 10 epochs for both the SM-VSF and CI-VSF variants using Mean Square Error Loss on the final image using the Adam Optimiser

and learning rate of 0.0001. We also did not use masking during the finetuning stage.

**Performance** Larger version of comparison of forecasted images downstream task is present in Figure 11

Received 20 February 2007; revised 12 March 2009; accepted 5 June 2009